Transport in semiconductor nanowire superlattices described by coupled quantum mechanical and kinetic models

2013 J. Phys.: Condens. Matter 25 335301

(http://iopscience.iop.org/0953-8984/25/33/335301)

IOP PUBLISHING JOURNAL OF PHYSICS: CONDENSED MATTER

J. Phys.: Condens. Matter **25** (2013) 335301 (10pp) doi:10.1088/0953-8984/25/33/335301

Transport in semiconductor nanowire superlattices described by coupled quantum mechanical and kinetic models

M Alvaro[1], L L Bonilla[1], M Carretero[1], R V N Melnik[1,2] and S Prabhakar[2]

[1] Gregorio Millán Institute for Fluid Dynamics, Nanoscience and Industrial Mathematics, Universidad Carlos III de Madrid, Avenida de la Universidad 30, E-28911 Leganés, Spain
[2] M^{2}NeT Lab, Wilfrid Laurier University, Waterloo, 75 University Avenue West, ON, N2L 3C5, Canada

E-mail: mariano.alvaro@uc3m.es

Received 1 March 2013, in final form 23 May 2013
Published 23 July 2013
Online at stacks.iop.org/JPhysCM/25/335301

Abstract

In this paper we develop a kinetic model for the analysis of semiconductor superlattices, accounting for quantum effects. The model consists of a Boltzmann–Poisson type system of equations with simplified Bhatnagar–Gross–Krook collisions, obtained from the general time-dependent Schrödinger–Poisson model using Wigner functions. This system for superlattice transport is supplemented by the quantum mechanical part of the model based on the Ben-Daniel–Duke form of the Schrödinger equation for a cylindrical superlattice of finite radius. The resulting energy spectrum is used to characterize the Fermi–Dirac distribution that appears in the Bhatnagar–Gross–Krook collision, thereby coupling the quantum mechanical and kinetic parts of the model. The kinetic model uses the dispersion relation obtained by the generalized Kronig–Penney method, and allows us to estimate radii of quantum wire superlattices that have the same miniband widths as in experiments. It also allows us to determine more accurately the time-dependent characteristics of superlattices, in particular their current density. Results, for several experimentally grown superlattices, are discussed in the context of self-sustained coherent oscillations of the current density which are important in an increasing range of current and potential applications.

(Some figures may appear in colour only in the online journal)

1. Introduction

Semiconductor superlattices (SSLs) can be produced by various techniques, among which sputtering and molecular-beam epitaxy remain the most common. Applications of SSLs include, but are not limited to, various nanolasers [1, 2], frequency generators and detectors [3–5], thermoelectrics-based nanostructures [6, 7], as well as a wide range of different optoelectronic devices [8–10].

Our main interests here lie with the III–V compound GaAs/AlAs SSLs, as it is well known that the difference in lattice constants between these materials is small and no residual stresses and strain appear. More precisely, we are interested in an adequate description of electronic transport in these low-dimensional nanostructures such that the quantum mechanical information is coupled to semiclassical models of the kinetic type. Both strongly coupled (when barriers are narrow) and weakly coupled (when barriers are wide) superlattices are of practical interest and the methodology developed in this work can be applied to both situations.

First we recall that for low electric fields the charge transport in doped SSLs can usually be described by semiclassical models for the motion of electrons in the lowest energy miniband, which is the only populated one (e.g., [11]). If Δ is the miniband width, Γ is the scattering width, eF the force due to the electric field ($-e < 0$ is the charge of the electron) and l the superlattice period, then this semiclassical

approach is considered to be a reasonable approximation if

$$\Delta \gg \Gamma, \qquad \Delta \gg eFl, \tag{1}$$

although comparisons with experiments frequently suggest that further corrections of semiclassical models may be necessary even in such situations. In the meantime, a direct comparison of the results from semiclassical models with the full quantum transport models, based on the nonequilibrium Green–Keldysh [11–13], Wigner functions [14, 15] or other approaches, remains a highly non-trivial (and partly elusive) task, from both fundamental and computational points of view. Furthermore including quantum mechanical information in semiclassical models becomes absolutely essential when condition (1) is violated. Therefore, in order to be able to describe the entire spectrum of the above situations, it is most natural to seek an efficient methodology for combining the quantum mechanical and semiclassical models.

One of our motivations here has been stimulated by the expanding areas of applications of coherent oscillations and localization phenomena. Indeed, the development of excitation of semiconductors is closely related to the field of coherent control of quantum dynamics (e.g., [16] and references therein). Different patterns of coherent oscillations of electrons provide a rich source of phenomena with far-reaching practical consequences. Examples of such oscillations in SSLs include both low-frequency oscillations (such as Gunn oscillations [17–19]) and high-frequency oscillations (such as Bloch oscillations [2]). Special conditions must exist in order to observe the latter class of oscillations. One of them is long scattering times, and SSLs are excellent candidates to satisfy this condition due to the fact that scattering is highly suppressed because of the spatial confinement, leading to a longer decoherence time. Low-dimensional nanostructures such as nanowire superlattices can provide a further advantage due to their lack of traverse excitations (present in quantum well superlattices), which eliminate this source of damping. Another interesting example of this type is quantum-dot superlattices, which have recently been studied in [20] for high (dc) electric fields. These objects are difficult to study, as coherent oscillations compete with dynamic localization under the influence of electric and/or magnetic fields. Other types of conditions that are usually required are special laws of collisions (e.g., inelastic collisions are often assumed in such studies). The benefits are well known and include gain at very high frequencies (THz) [8], as well as resonance peaks in the absorption coefficients. Recent studies demonstrated a series of important advantages in other types of Bloch oscillations, such as magnetic [21] and surface acoustic Bloch oscillations [22].

In this work, our quantum mechanical/semiclassical approach in studying coherent oscillations and other transport phenomena in low-dimensional nanostructures, focusing on SSLs, will be exemplified for one-miniband SSLs. Miniband structures of SSLs have been studied extensively since the works of Esaki and Tsu on transport in these structures, and experimental results have frequently provided a good guideline for further theoretical progress and applications in the area [3, 23]. Whenever required, extensions to multiple minibands can be developed based on the Wigner function description and the $\mathbf{k} \cdot \mathbf{p}$ theory (e.g., [24–27]). While semiclassical models continue to play an important role in these studies, the importance of the quantum mechanical part in the analysis of miniband structures of periodic superlattices was emphasized already 20 years ago (e.g., [28] and references therein). Today, the interest in the development of methods capable of combining quantum mechanical and semiclassical models is fueled by both open fundamental questions and practical applications (e.g., [29] and references therein).

Early developments were limited to quantum corrections of semiclassical models constructed on the basis of relaxation-time approximations [30–32]. Currently such models span the entire hierarchy of relaxation-time approximations, from quantum drift-diffusion models [33], to various types of hydrodynamic models [34], and to quantum-kinetic models [15]. Rigorous reduction procedures between such models have also been derived. For example, starting from the semiclassical Boltzmann–Poisson models we can arrive at various types of hydrodynamic models, as well as nonlocal drift-diffusion equations [34, 35].

In what follows, we are interested in the kinetic type models in this hierarchy, in particular in the Wigner–Poisson (WP) model. The latter is a relaxation-time model which is equivalent to the von Neumann–Poisson (or quantum Liouville–Poisson) model for the time evolution of the density matrix and describing open quantum mechanical systems with relaxation mechanisms [36]. We use the WP model and its semiclassical limit, the Boltzmann–Poisson model, to describe transport in a nanowire superlattice (NWSL). The collision model has a 1D elastic impurity collision term as in [30] and a relaxation-time term with a local equilibrium distribution having the same electron density as the actual distribution function (in our case, the local distribution function is Fermi–Dirac, not Boltzmann-type as in [31]). With respect to the usual multi-quantum well SSL having a very large cross section, the NWSL has cylindrical cross section with small radius. The dispersion relation is parabolic with respect to a quantized transversal wave vector, thus changing the local equilibrium distribution function.

The advantage of the collision model we use compared to the usual integral terms in the Boltzmann equation is its simplicity, which renders the kinetic equation amenable to perturbation calculations such as the Chapman–Enskog procedure [15] and computationally cheaper to solve. In our model, the two collision frequencies (or reciprocal collision times) are assumed to be constant for simplicity. They can be selected by comparing the field and the velocity at the maximum of the drift velocity versus field curve with data obtained from numerical solutions of the Boltzmann equation, the nonequilibrium Green function theory [11] or experiments [37] (see also calculations of scattering times in the case of a weakly coupled SSL in [38]). This calibration is easy if there is an analytical expression for the drift velocity [31], which, in turn, is used in a simple drift-diffusion

model as in [37]. For our model of the NWSL, we have not found such an expression and therefore we would require numerical computations to select optimal values of the collision frequencies. Here we adopt indicative values for the collision frequencies similar to those used in experiments with SSL having large cross sections [37]. The rest of the paper is as follows. In section 2, we provide details of the kinetic part of the model. Starting from the time-dependent Schrödinger–Poisson (TDSP) model we highlight how it can be reduced to the WP equations or the Boltzmann–Poisson type system for carrier transport in the lowest miniband of a SSL. We discuss the main advantages of this approach. In section 3, we give details of the quantum mechanical part of the model and the mechanism of its coupling to the kinetic part via the Fermi–Dirac distribution. In this section we also discuss dispersion relations for three representative experimentally grown examples of SSLs. In section 4, we discuss the results obtained with the developed model and compare them with those obtained with conventional models. The differences are highlighted for oscillation frequencies and amplitudes of the total current density. Conclusions are given in section 5.

2. Schrödinger–Poisson models and the Wigner–Poisson approach to superlattice transport

Time-dependent models, based on quantum Liouville or Schrödinger equations, provide a unifying framework for the description of electronic transport in low-dimensional semiconductor nanostructures. The relationship between such models and the Schrödinger–Poisson system, as well as the Wigner–Poisson system, is well elucidated in the literature (e.g., [39, 40] and references therein). The connection between the latter two systems is also known. Indeed, under appropriate assumptions, a mixed state system of TDSP type is equivalent to the WP system. The well-posedness of the WP system has also been studied extensively [41].

The simplest TDSP model describing electrons interacting through their self-consistent Hartree potential reads as follows:

$$\mathrm{i}\hbar\frac{\partial\Psi}{\partial t} = -\frac{\hbar^2}{2m}\Delta\Psi + V(\Psi)\Psi, \tag{2}$$

$$\varepsilon\Delta V(\Psi) = -en, \tag{3}$$

where $-e < 0$ is the electron charge, $\Psi = (\psi_m)_{m\in\mathbb{N}}$ is the wave function, ε is the dielectric permittivity, V is the potential, and the electron concentration is given by

$$n(x,t) = \sum_m \lambda_m \parallel \psi_m(x,t)\|^2. \tag{4}$$

Here the λ_m are coefficients (eigenvalues) in the density matrix representation of the system in $(x,t) \in \mathbb{R}^3 \times (0,+\infty)$ under consideration:

$$\rho = \sum_m \lambda_m P_m, \tag{5}$$

so that the operator ρ is assumed to be positive and self-adjoint, while the P_m are projections onto the subspace spanned by the eigenvectors associated with λ_m. Charge transport in a SSL is more complicated as one needs to include also the periodic potential which gives rise to the electron minibands and a scattering potential, phonon–electron interactions, etc. Once the electronic structure is considered, the quantum (WP) kinetic model may be derived from the band SP system by using the Wigner function in the form:

$$w_{\mu,\nu}(\mathbf{x},\mathbf{k},t) = \int \rho_{\mu,\nu}(\mathbf{x}+\tfrac{1}{2}\xi, \mathbf{x}-\tfrac{1}{2}\xi, t)\mathrm{e}^{\mathrm{i}\mathbf{k}\cdot\xi}\,\mathrm{d}\xi, \tag{6}$$

where the band density matrix, for minibands μ and ν, is defined by

$$\rho_{\mu,\nu}(\mathbf{x},\mathbf{y},t) = \langle\Psi_\mu^\dagger(\mathbf{x},t)\Psi_\nu(\mathbf{y},t)\rangle. \tag{7}$$

To find an equation for $w(\mathbf{x},\mathbf{k},t) = \sum_{\mu,\nu} w_{\mu,\nu}(\mathbf{x},\mathbf{k},t)$, we assume that only the first miniband is populated and that there are no transitions between minibands, i.e. $w(\mathbf{x},\mathbf{k},t) \approx w_{1,1}(\mathbf{x},\mathbf{k},t)$. Then, we obtain the following evolution equation for the periodic Wigner function $f = w(\mathbf{x},\mathbf{k},t)$ [15]:

$$\begin{aligned}\frac{\partial}{\partial t}f + \frac{\hbar\mathbf{k}_\perp}{m^*}\cdot\frac{\partial}{\partial\mathbf{x}_\perp}f + \frac{\mathrm{i}}{\hbar}\sum_{m=-\infty}^{\infty}\mathrm{e}^{\mathrm{i}mkl}E_{1m}(\mathbf{k}_\perp)[f(x\\ + ml/2,\mathbf{x}_\perp,\mathbf{k},t) - f(x-ml/2,\mathbf{x}_\perp,\mathbf{k},t)]\\ + \frac{\mathrm{i}e}{\hbar}\left[V\left(x+\frac{1}{2\mathrm{i}}\frac{\partial}{\partial k},\mathbf{x}_\perp\right)\right.\\ \left. - V\left(x-\frac{1}{2\mathrm{i}}\frac{\partial}{\partial k},\mathbf{x}_\perp\right)\right]f = Q[f],\end{aligned} \tag{8}$$

where $f(\mathbf{x},k+\frac{2\pi}{l},\mathbf{k}_\perp,t) = f(\mathbf{x},k,\mathbf{k}_\perp,t)$, $\mathbf{k} = (k,\mathbf{k}_\perp)$, V is the electric potential, $Q[f]$ is the collision term and $l = L_\mathrm{b} + L_\mathrm{w}$ is the SSL period of a SSL with barrier and well widths of L_b and L_w, respectively. The energy of the first miniband is given by:

$$E_1(\mathbf{k}) = \sum_{m=-\infty}^{\infty} E_{1m}(\mathbf{k}_\perp)\,\mathrm{e}^{\mathrm{i}mkl}.$$

The electric field $-\mathbf{F} = -\partial W/\partial\mathbf{x}$ satisfies the Poisson equation:

$$\varepsilon\left(\frac{\partial F}{\partial x} + \frac{\partial}{\partial\mathbf{x}_\perp}\cdot\mathbf{F}_\perp\right) = \frac{e}{l}(n - N_D), \tag{9}$$

and the two-dimensional (2D) electron density is:

$$\begin{aligned}&n(x,\mathbf{x}_\perp,t)\\ &= \frac{l}{4\pi^3}\int_{-\pi/l}^{\pi/l}\int_{-\infty}^{\infty}\int_{-\infty}^{\infty} f(x,\mathbf{x}_\perp,k,\mathbf{k}_\perp,t)\,\mathrm{d}k\,\mathrm{d}\mathbf{k}_\perp.\end{aligned} \tag{10}$$

The collision term in the resulting (WP) model (8)–(9) is given here by the approximation:

$$Q[f] \equiv -\nu_\mathrm{en}(f - f^\mathrm{FD}) - \nu_\mathrm{imp}\frac{f(k)-f(-k)}{2}, \tag{11}$$

where f^FD is the Fermi–Dirac local equilibrium distribution producing the same electron density as the Wigner function, $1/\nu_\mathrm{en}$ represents the inelastic collisions relaxation time and $1/\nu_\mathrm{imp}$ is the relaxation time for elastic collisions such as impurity scattering [30], which conserve energy but

dissipate momentum (transfer of lateral momentum due to impurity scattering [42] is neglected in (8)–(11)). Relaxation to a Boltzmann local equilibrium (instead of Fermi–Dirac) produces a simplified form of the Bhatnagar–Gross–Krook collision model, first used by Ignatov and Shashkin to describe self-sustained oscillations in SSLs [31].

The WP model (8)–(9) can be viewed as a phase-space counterpart of the Schrödinger–Poisson systems [43], which have also been analyzed extensively, under various mathematical assumptions (e.g., [44, 45] and references therein). This phase-space representation of a quantum mechanical system has an advantage of relatively easy comparisons with its classical counterparts.

The WP system can also be viewed as the quantum analogue of the well-known Vlasov–Poisson model, describing a spatially inhomogeneous collisionless plasma. In this system the acceleration term is given by a pseudo-differential operator, replacing the classical differential operator in the Boltzmann equation. In the (semi-)classical limit, the WP system is reduced to the Vlasov–Poisson, while in the case of collisions these systems can be generalized depending on the collision law to, for example, the Vlasov–Poisson–Fokker–Planck and Wigner–Poisson–Fokker–Planck in the classical and quantum mechanical case, respectively [46]. They can serve as a basis for deriving 'lower order' models in the modeling hierarchy by using various expansion methodologies (e.g., Hilbert, Chapman–Enskog, spherical harmonic expansions, singular perturbation techniques, etc).

We suppose that the Wigner function does not depend on $\mathbf{x}_\perp$ and define the 1D Wigner function by:

$$f(x,k,t) = \frac{1}{2\pi^2 S}\int\int f(x,\mathbf{x}_\perp,k,\mathbf{k}_\perp,t)\,\mathrm{d}\mathbf{k}_\perp\,\mathrm{d}\mathbf{x}_\perp, \quad (12)$$

where S is the superlattice cross section. In the semiclassical limit, the pseudo-differential operators in the left hand side of (8) become the usual convective terms and we obtain the following Boltzmann–Poisson system for carrier transport in the lowest miniband of SSLs (see [34] and references therein):

$$\frac{\partial f}{\partial t} + v(k)\frac{\partial f}{\partial x} + \frac{eF}{\hbar}\frac{\partial f}{\partial k} = -\nu_{en}(f - f^{\mathrm{FD}}) - \nu_{\mathrm{imp}}\frac{f(k)-f(-k)}{2}, \quad (13)$$

$$F = \frac{\partial V}{\partial x}, \qquad v(k) = \frac{1}{\hbar}\frac{\mathrm{d}\mathcal{E}}{\mathrm{d}k}, \quad (14)$$

$$\varepsilon\frac{\partial^2 V}{\partial x^2} = \frac{e}{l}(n - N_{\mathrm{D}}), \quad (15)$$

$$n(x,t) = \frac{l}{2\pi}\int_{-\pi/l}^{\pi/l} f(x,k,t)\,\mathrm{d}k = \frac{l}{2\pi}\int_{-\pi/l}^{\pi/l} f^{\mathrm{FD}}(k;\mu(n))\,\mathrm{d}k, \quad (16)$$

$$J(t) = \frac{1}{L}\int_0^L J_n(x,t)\,\mathrm{d}x, \qquad J_n = \frac{e}{2\pi}\int_{-\pi/l}^{\pi/l} v(k) f(x,k,t)\,\mathrm{d}k, \quad (17)$$

with $x \in [0, L]$ and f periodic in k with period $2\pi/l$. Here f, f^{FD}, n, N_D, $\mathcal{E}$, l, L, $-F$, ε, μ, $-e < 0$, J_n and J are the one-particle distribution function, the 1D local equilibrium distribution function, the 2D electron density, the 2D doping density, the miniband dispersion relation, the SSL period, the SSL length, the electric field, the SSL permittivity, the chemical potential, the electron charge, the current density and the total current density, respectively. Both the exact and the local equilibrium Fermi–Dirac distribution functions have the same electron density according to (16).

This model has a number of advantages compared to other existing models. First, it is known that, with a general local equilibrium distribution, it is suitable for the description of Bloch and Gunn type oscillations [34], among other important phenomena. Second, despite the fact that the model is quite general, it is computationally manageable to be applied in fundamental studies and for practical applications. At the same time, the model requires adequate approximations of $v(k)$ and f^{FD}, which will be discussed in section 3.

3. Quantum mechanical part of the model

Two main characteristics entering the model (13)–(17) account for quantum effects. They are $v(k)$ and f^{FD}. We start from the group velocity, which can be determined as

$$v(k) = \frac{1}{\hbar}\frac{\mathrm{d}\mathcal{E}(k)}{\mathrm{d}k}. \quad (18)$$

The frequently used approximation to the dispersion relation

$$\mathcal{E}(k) = \frac{\Delta}{2}[1 - \cos(kl)], \quad (19)$$

where Δ is the first miniband width, may not always be appropriate. Indeed, this 'tight-binding' approximation is usually obtained under the assumption of a large barrier thickness. In this case states are practically dispersionless and uncoupled, while tunneling with respect to them can be treated as a small perturbation. They are fully confined, leading to a dispersion relation which is periodic with period $2\pi/l$ and fully sinusoidal.

A more general approach to obtain the dispersion relation, which would provide a better approximation than (19), is to start directly from the Hamiltonian of the SSL under consideration and solve the Schrödinger equation, given in the Ben-Daniel–Duke form [47]:

$$-\frac{\hbar^2}{2}\nabla\cdot\left[\frac{1}{m(\mathbf{r})}\nabla\Psi(\mathbf{r})\right] + V(\mathbf{r})\Psi(\mathbf{r}) = E\Psi(\mathbf{r}). \quad (20)$$

As before, here $V(\mathbf{r})$ is the potential, E is the eigenenergy of the SSL, $m(\mathbf{r})$ is the effective mass, while the wave function is given as $\Psi(\mathbf{r}) = \psi(r,\phi,z) = \Phi(\phi)J(r)Z(z)$. The analysis of miniband structures of SSLs with arbitrary periodic potential profiles is only possible based on numerical methods, and both finite element and finite difference methods can be used for this purpose [47–49]. If a superlattice structure has cylindrical symmetry, a computationally inexpensive Generalized Kronig–Penney model (G.K–P approximation)

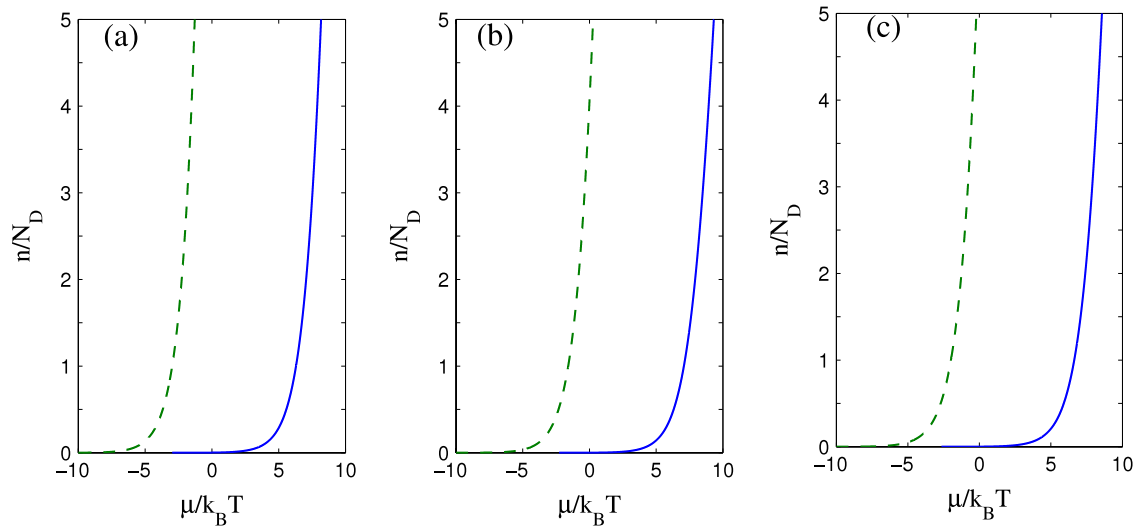

Figure 1. Nondimensional electron density versus chemical potential for the 16 meV (a), 43 meV (b) and 72 meV (c) superlattices of table A.2, at $T = 300$ K. The solid line represents that radial effects are considered in the Fermi–Dirac local equilibrium distribution. The dashed line means that the dispersion relation is computed with the Kronig–Penney model for an infinite superlattice.

for such structures has been developed. Following [47], we have two equations to be solved numerically:

$$r\frac{\mathrm{d}}{\mathrm{d}r}\left(r\frac{\mathrm{d}J}{\mathrm{d}r}\right) + (q^2r^2 - \tilde{l}^2)J(r) = 0, \tag{21}$$

$$\frac{\mathrm{d}}{\mathrm{d}z}\left[\frac{1}{m(z)}\frac{\mathrm{d}Z(z)}{\mathrm{d}z}\right] + \frac{2}{\hbar^2}\left[E - V(z) - \frac{\hbar^2\gamma^2_{\tilde{l},\tilde{n}}}{2m(z)R_0^2}\right]Z(z) = 0, \tag{22}$$

while the solution of the third, angular one, is given by $\Phi(\phi) = \exp(\pm \mathrm{i}\tilde{l}\phi)$. The solution of (21) is a Bessel function of the first kind, where the quantum number q satisfies the boundary condition $J(qR_0) = 0$, with R_0 being the SSL radius, $\gamma_{\tilde{l},\tilde{n}} = qR_0$. The solution of (22) can be dealt with using a computationally inexpensive Generalized Kronig–Penney model (G.K–P approximation) for the infinitely long SSL, which leads to the solution of the following nonlinear equation:

$$\cos kl = \cos(k_\mathrm{w}L_\mathrm{w})\cosh(k_\mathrm{b}L_\mathrm{b}) + \frac{k_\mathrm{b}^2m_\mathrm{w}^2 - k_\mathrm{w}^2m_\mathrm{b}^2}{2k_\mathrm{w}k_\mathrm{b}m_\mathrm{b}m_\mathrm{w}}\sin(k_\mathrm{w}L_\mathrm{w})\sinh(k_\mathrm{b}L_\mathrm{b}), \tag{23}$$

where, as before, $l = L_\mathrm{b} + L_\mathrm{w}$, while k_b, m_b, V and k_w, m_w, 0, are wave numbers, electron effective masses and potential energies in the barrier and well, respectively:

$$k_\mathrm{b} = \left[\frac{2m_\mathrm{b}(\mathcal{V} - \mathcal{E})}{\hbar^2}\right]^{\frac{1}{2}}, \qquad k_\mathrm{w} = \left[\frac{2m_\mathrm{w}\mathcal{E}}{\hbar^2}\right]^{\frac{1}{2}}, \tag{24}$$

$$\mathcal{E} = E - \frac{\hbar^2q^2}{2m_\mathrm{w}}, \qquad \mathcal{V} = V + \frac{\hbar^2q^2}{2m_\mathrm{b}} - \frac{\hbar^2q^2}{2m_\mathrm{w}}, \qquad q = \frac{\gamma_{\tilde{l},\tilde{n}}}{R_0}. \tag{25}$$

The solutions of (23) are the 1D miniband energies $\mathcal{E}_\nu(k, \gamma_{\tilde{l},\tilde{n}})$, $\nu = 1, 2, \ldots$. Then the energy of the first miniband of the cylindrical NWSL is:

$$E_1 = \mathcal{E}_1(k, \gamma_{\tilde{l},\tilde{n}}) + \frac{\hbar^2\gamma^2_{\tilde{l},\tilde{n}}}{2m_\mathrm{w}R_0^2}, \tag{26}$$

where m_w is the electron effective mass at the well. Therefore, the Fermi–Dirac local equilibrium distribution function becomes:

$$f^\mathrm{FD} = \frac{2}{\pi R_0^2}\sum_{\tilde{l},\tilde{n}=0}^{\infty}\frac{1}{1 + \exp\left(\frac{\mathcal{E}_1 - \mu}{k_\mathrm{B}T} + \frac{\hbar^2\gamma^2_{\tilde{l},\tilde{n}}}{2m_\mathrm{w}R_0^2k_\mathrm{B}T}\right)}, \tag{27}$$

where μ is the chemical potential and T is the SSL temperature. The above Fermi–Dirac distribution function provides coupling between the kinetic WP part of the model (8)–(11) and its quantum mechanical part (21)–(22). The minimum number of zeros of the Bessel function necessary for the convergence of the series in (27) is calculated in table A.1 as a function of the nondimensional parameter $\frac{\hbar^2}{2m_\mathrm{w}R_0^2k_\mathrm{B}T}$. We can compare (27) with the local equilibrium distribution obtained when the SSL cross section is infinite (the common case of a quantum well SSL):

$$f^\mathrm{FD} = \frac{m^*k_\mathrm{B}T}{\pi\hbar^2}\ln\left[1 + \exp\left(\frac{\mu - \mathcal{E}_1}{k_\mathrm{B}T}\right)\right], \tag{28}$$

where $m^* = (m_\mathrm{w}L_\mathrm{w} + m_\mathrm{b}L_\mathrm{b})/l$. In figure 1 we present the results of comparisons between the electron densities computed with (16) for both Fermi–Dirac local equilibrium distribution functions (27) and (28) for the three experimentally grown superlattices (their characteristics are given in table A.2, at $T = 300$ K). Next, we provide a detailed analysis of dispersion relations for these superlattices that cover a range of experimentally grown SSLs.

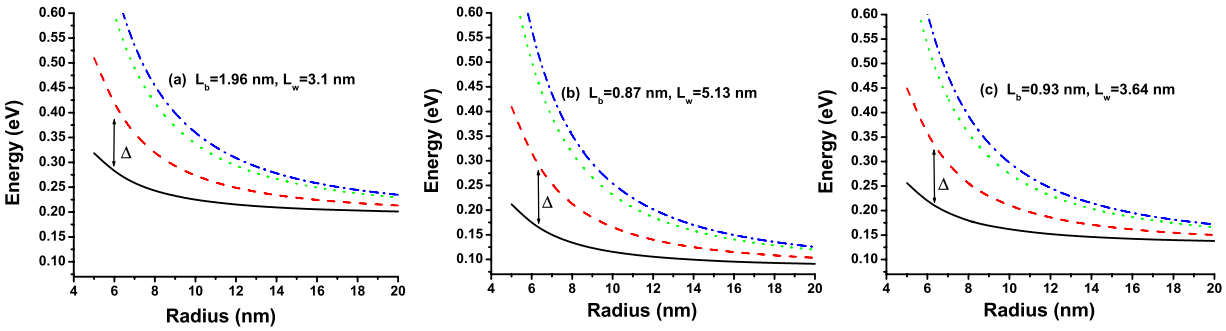

Figure 2. Four lowest miniband energies versus the radius of the GaAs/AlAs nanowire superlattice at $k = 0$. We chose the following parameters: $m_w = 0.0665m_0$, $m_b = 0.15m_0$, $V_b = 0.982$ eV. Miniband energies are determined by using the condition $\mathcal{J}_{\tilde{l}}(qR_0) = 0$ (see details in the text).

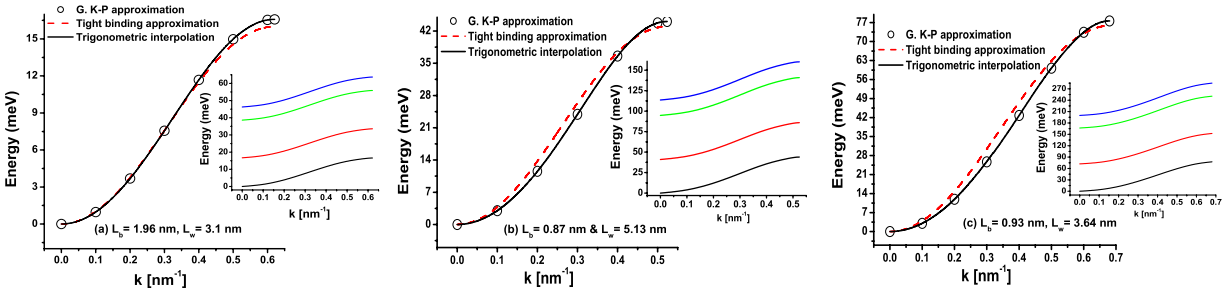

Figure 3. Dispersion relation for the lowest miniband: energy versus k for the GaAs/AlAs nanowire superlattice. Inset: dispersion relation for the four lower minibands. The radii of the nanowires are $R = 17$ nm (a), which corresponds to the miniband width 16 meV; $R = 11$ nm (b), which corresponds to the miniband width 43 meV, and $R = 8.2$ nm (c), which corresponds to the miniband width 72 meV (see table A.2). Solid lines show the data from the trigonometric interpolation, which is in excellent agreement with the data obtained from the G.K–P method.

As mentioned in section 1, both weakly and strongly coupled superlattices are of substantial practical interest. Based on [37], we consider three representative examples of experimentally grown GaAs/AlAs SSLs (see corresponding rows 1, 3, and 6 in table 1 of [37]):

- SSL 1: $L_b = 1.96$ nm, $L_w = 3.1$ nm with $\Delta = 16$ meV;
- SSL 2: $L_b = 0.87$ nm, $L_w = 5.13$ nm with $\Delta = 43$ meV;
- SSL 3: $L_b = 0.93$ nm, $L_w = 3.64$ nm with $\Delta = 72$ meV.

SSL 1 is closer to the case of weakly coupled superlattices, while SSL 2 and SSL 3 correspond to the case of strongly coupled superlattices. Further details on the characteristics of these superlattices are given in table A.2 of the appendix.

The data obtained numerically from the application of the G.K–P methodology have been interpolated and the dispersion relation has been presented by the following trigonometric series:

$$\mathcal{E}(k) = \tfrac{1}{2}a_0 + \sum_{j=1}^{m}[a_j \cos(jkl) + b_j \sin(jkl)], \qquad (29)$$

where $l = L_b + L_w$ and the coefficients a_j and b_j used in the approximations for all three superlattices are summarized in the appendix in tables A.3–A.5, respectively.

Based on model (23) solved for $k = 0$, in figure 2 we present four lowest miniband energies as functions of the radius of GaAs/AlAs superlattices that correspond to the three cases of SSLs considered above. Here we use also the boundary condition for the radial equation $\mathcal{J}_{\tilde{l}}(qR_0) = 0$ (e.g., $qR_0 = 0.240\,48$ for the first zero of $\mathcal{J}_0$, $qR_0 = 3.8317$ for the first zero of $\mathcal{J}_1$, and similarly for the third and fourth minibands). The wave numbers in the barrier and well are defined in (24)–(25). Note that, given the miniband width, it is straightforward to determine the radius of the corresponding SSL (see inserts of figure 3). In figure 3 the dispersion relations, obtained by the G.K–P methodology, are given for our three cases. They are compared with the simple 'tight-binding' approximations (see (19)). The curves corresponding to the dispersion relations, obtained with the trigonometric interpolation (29), are also given.

The developed methodology allows us to find the radii of the nanowire superlattices that have the same miniband widths as those in the experiments of [37]. The G.K–P model approximates a SSL with a given number of periods by calculating the minibands of a SSL with infinitely many periods. We can compare the results produced by the G.K–P approximation with the complete quantum mechanical solution of the Schrödinger equation that determines the spectra of the corresponding superlattices with finitely many quantum wells:

$$-\frac{\hbar^2}{2}\frac{\partial}{\partial z}\left(\frac{1}{m(z,r)}\frac{\partial \chi_{\tilde{l}}}{\partial z}\right) - \frac{\hbar^2}{2r}\frac{\partial}{\partial r}\left(\frac{r}{m(z,r)}\frac{\partial \chi_{\tilde{l}}}{\partial r}\right) + \frac{\hbar^2}{2m(z,r)}\frac{\tilde{l}^2}{r^2}\chi_{\tilde{l}}(r,z) + V(z,r)\chi_{\tilde{l}}(r,z) = E\chi_{\tilde{l}}(r,z). \qquad (30)$$

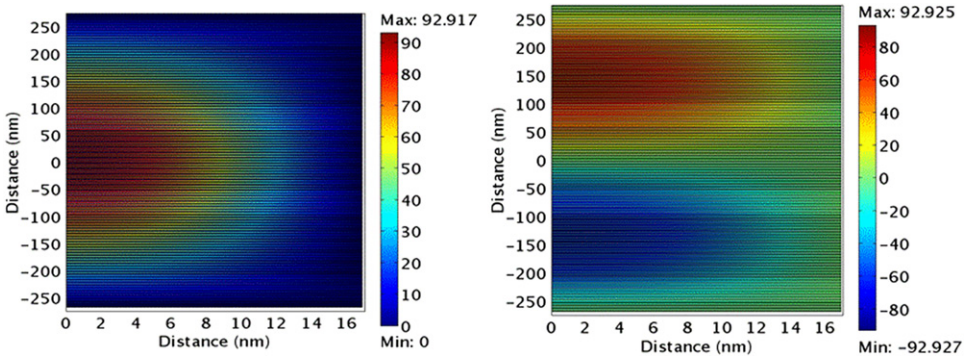

Figure 4. Ground and first excited state of the wave function of electrons in a symmetric AlAs/GaAs superlattices nanostructure (with the number of periods 109, $R = 17$ nm and $\tilde{l} = 0$). Eigenvalues for the ground and first excited states are $E_1 = 0.204\,249$ eV and $E_2 = 0.204\,258$ eV. The vertical and horizontal axes represent the nanowire SSL longitudinal and radial distance, respectively.

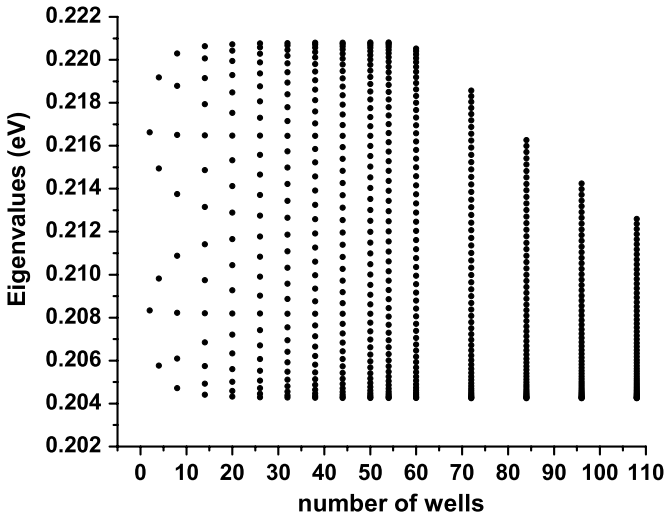

Figure 5. Formation of minibands in GaAs/AlAs superlattices: eigenvalues versus the number of superlattice periods. The discrete energy states converge to the continuum spectrum as the number of periods becomes sufficiently large.

Here both the potential and the effective mass can be a function of both z and r and where $\Psi(r, \phi, z) = \Phi(\phi)\chi_{\tilde{l}}(r, z)$. Such solutions are obtained with the finite element method, and a representative example is given in figure 4. Both the ground state and the first excited state energies are presented for the case that corresponds to SSL 1. Finally, in figure 5 we present the formation of the miniband structure in this superlattice as we increase the number of periods to demonstrate the convergence to the continuum situation that would allow us to proceed next to the semiclassical part of the model.

4. Results and discussion

Having determined the quantum mechanical input for the kinetic model, we are moving to the numerical solution of system (13)–(17). In recent years, several groups have been attempting to solve the Wigner–Poisson system directly (e.g., [50] and references therein). However, in most cases, such approaches have been using heuristic information for the quantum mechanical part.

Our focus is on the solution (13)–(17) for the case of the three different superlattices considered in section 3. In what follows, we have used the numerical parameters given in table A.2, corresponding to the superlattices SSL 1, SSL 2, and SSL 3, providing a good representative sampling range of experimentally grown superlattices.

The kinetic part of the model (13)–(17) has been solved by an implicit finite difference scheme, with the following initial conditions:

$$f(x, k, 0) = f^{(0)}(x, k, 0) \tag{31}$$

$$F(x, 0) = V_{\text{bias}}/L \tag{32}$$

and the following Ohmic boundary conditions at the contacts:

at $x = 0$:

$$f^{+} = \frac{2\pi\hbar\sigma F}{e\Delta} - \frac{f^{(0)}}{\int_0^{\frac{\pi}{l}} v(k) f^{(0)}\,\mathrm{d}k} \int_{-\frac{\pi}{l}}^{0} v(k) f^{-}\,\mathrm{d}k, \tag{33}$$

at $x = L$:

$$f^{-} = \frac{2\pi f^{(0)}}{l \int_{-\frac{\pi}{l}}^{0} f^{(0)}\,\mathrm{d}k} \left(N_D - \frac{l}{2\pi} \int_0^{\frac{\pi}{l}} f^{+}\,\mathrm{d}k \right), \tag{34}$$

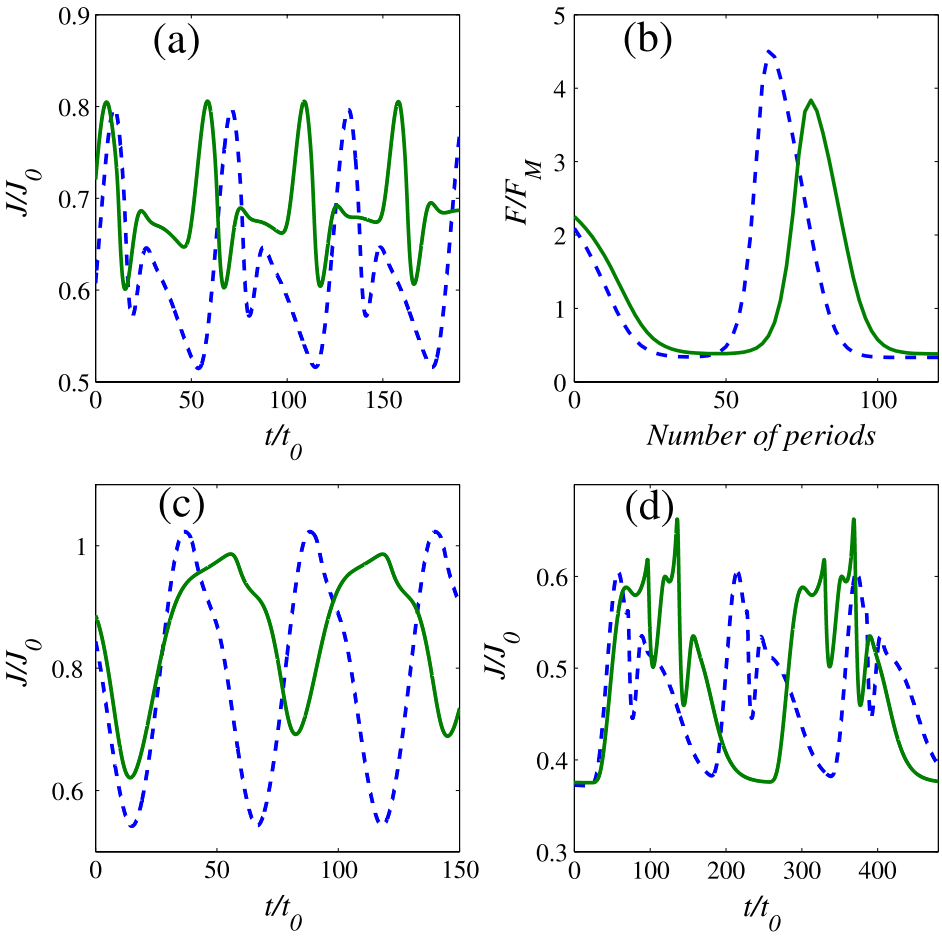

Figure 6. (a) Current density versus time during self-sustained current oscillations for the 72 meV superlattice. (b) Fully developed dipole wave moving from the cathode to the anode during self-sustained current oscillations. (c) and (d) Same as (a) for the 16 meV and 43 meV superlattices, respectively. The solid line indicates that the finite radius effects are taken into account. The dashed line represents that the dispersion relation is computed with the Kronig–Penney model for an infinite superlattice. The initial transients are not shown for clarity. To transform the magnitudes in this figure to dimensional units, use table A.2.

where V_{bias} is the constant applied voltage bias, σ is the contact conductivity, $f^{\pm}$ means $f(x, k, t)$ for $\text{sign}(k) = \pm 1$ and $f^{(0)}$ is the leading order approximation for the distribution function in the Chapman–Enskog expansion, e.g. $f^{(0)}$ is the solution of (13) when we drop the x and t derivatives of f. We also need the constant voltage bias condition:

$$\int_0^L F(x, t)\, \mathrm{d}x = V_{\text{bias}}. \tag{35}$$

In figure 6 and table 1 we summarize our findings. We have compared the results obtained with our kinetic model, which takes into account quantum mechanical effects and a finite superlattice radius, and the results obtained using the conventional approximation of the dispersion relation based on the standard Kronig–Penney model for an infinite superlattice. While in the latter case the transversal effects are neglected (f^{FD} is (28)) and the 'tight-binding' dispersion relation (19) is used, in the former case we use the refined approximations (29) and (27) that couple the kinetic and quantum mechanical parts of the model.

For appropriate values of the voltage V_{bias} there are solutions having the form of self-sustained oscillations of the current. In all cases, these oscillations are due to the periodic motion and recycling of charge dipole waves, as shown in figure 6(b). Table 1 compares the frequency and current density amplitude of nanowire superlattices with finite radii to those having infinite radii. We have estimated the elastic (1.2×10^{13} s^{-1}) and inelastic (1.32×10^{13} s^{-1}) scattering rates by comparing numerical simulations of the model to the available frequencies from experiments [37]. To calibrate the electron velocity of a drift-diffusion model for a SSL with tight-binding dispersion relation is simpler because one can use a well-known formula for the peak velocity [37]. An alternative way to estimate the scattering times is by using Monte Carlo simulations to calculate the superlattice current–voltage characteristics and infer the scattering times from the peak velocity formula [11]. For the 16 and 72 meV superlattices we have found that the frequency of the current oscillations is closer to the experimental value [37] when the finite radius effects are considered. However, for the 43 meV superlattice, the frequency of the oscillations is closer to the experimental value when the radial effects are not taken into account. This particular superlattice has a larger doping density, which yields a larger electron density when the

Table 1. Oscillation frequencies and amplitudes of the total current density obtained (a) with the coupled model including a finite radius, and (b) with the conventional kinetic model for a superlattice with infinite radius. The results are presented for the nanowire superlattices SSL 1, SSL 2, and SSL 3 with all parameters given in table A.2.

	Frequency (GHz)		Current density amplitude (10^4 A cm^{-2})	
Δ (meV)	Radial effects	Infinite SL	Radial effects	Infinite SL
16	2.36	3	0.15	0.20
43	10.5	16	1.5	1.4
72	53.4	43.2	1.6	2.2

dipole wave reaches the receiving contact. When the electron density increases, the velocity of the dipole wave decreases, producing a lower frequency of the oscillations. Our results are comparable to those obtained by Schomburg *et al* [37] using a simpler drift-diffusion model for SSL with an infinite cross section. However, when predicting the frequency of a similar superlattice with a 140 meV miniband width [4], our model for a SSL with infinite cross section predicts a frequency of 68 GHz, which is much closer to observations (70 GHz) than the estimation (∼125 GHz) found using the linear interpolation in figure 4 of [37].

5. Conclusions

In this paper we have developed a kinetic model for the analysis of semiconductor superlattices, accounting for quantum effects. The first part of the model is the conventional Boltzmann–Poisson system that is obtained from the general time-dependent Schrödinger–Poisson model via the Wigner approach. Collisions include a simplified version of the Bhatnagar–Gross–Krook relaxation-time model and a one-dimensional impurity collision term. The second part of the model is based on the Ben-Daniel–Duke form of the Schrödinger equation. The coupling between these two parts of the model is realized via the Fermi–Dirac distribution. The resulting model uses the dispersion relation obtained from the generalized Kronig–Penney method, and allows us to estimate radii of superlattices that have the same miniband widths as those used in experiments. The model has been solved numerically and results have been presented for a range of experimentally grown superlattices. Differences, induced by the finite radius effects, have been discussed in the context of self-sustained coherent oscillations of the current in such superlattices.

Acknowledgments

This work was supported by NSERC and CRC (Canada) and by MICINN Grant Nos FIS2008-04921-C02-01 and FIS2011-28838-C02-01 (Spain). This work was made possible by the facilities of the Canadian Shared Hierarchical Academic Research Computing Network (SHARCNET).

Appendix

See tables A.1–A.5

Table A.1. Minimum number of zeros of the Bessel function necessary for the convergence of the series in (27), calculated as a function of the nondimensional parameter $\frac{\hbar^2}{2m_w R_0^2 k_B T}$, corresponding to the nanowire superlattices SSL 1, SSL 2, and SSL 3, respectively.

$\frac{\hbar^2}{2m_w R_0^2 k_B T}$	16 meV mn	43 meV mn	72 meV mn
0.5	4	9	4
0.3	9	16	9
0.1	25	49	36
0.05	64	100	64
0.01	324	576	400

Table A.2. Parameters used for the numerical solution of the drift-diffusion equations for the nanowire superlattices in row 1, 3 and 6 of [37].

Δ (meV)	L_w (nm)	L_b (nm)	Length (μm)	N_D (10^{17} cm^{-3})	σ ($(\Omega$ m$)^{-1}$)	V_{bias} (V)	F_M (kV cm^{-1})	t_0 (ps)	J_0 (10^4 A cm^{-2})
16	3.1	1.96	0.55	0.8	14	1.51	22.6	6.3	0.41
43	5.13	0.87	0.60	1.4	50	1.14	19.1	0.39	5.58
72	3.64	0.93	0.64	1.0	90	1.58	25.1	0.37	7.7

Table A.3. Coefficients for the trigonometric interpolation for the nanowire superlattice SSL 1: $L_b = 1.96$ nm and $L_w = 3.1$ nm.

a_j (meV)	b_j (10^{-16} meV)	a_j (meV)	b_j (10^{-16} meV)
$a_0 = 16.2873$	—	$a_4 = 0.0002$	$b_4 = 0.0344$
$a_1 = -8.2888$	$b_1 = 0$	$a_5 = -0.0004$	$b_5 = 0.0489$
$a_2 = 0.1492$	$b_2 = -0.3648$	$a_6 = -0.0002$	$b_6 = 0.0914$
$a_3 = -0.0042$	$b_3 = -0.1027$	$a_7 = 0.0005$	$b_7 = 0.0609$

Table A.4. Coefficients for the trigonometric interpolation for the nanowire superlattice SSL 2: $L_b = 0.87$ nm and $L_w = 5.13$ nm.

a_j (meV)	b_j (10^{-15} meV)	a_j (meV)	b_j (10^{-15} meV)
$a_0 = 40.8898$	—	$a_4 = 0.0258$	$b_4 = 0.0329$
$a_1 = -21.8458$	$b_1 = 0$	$a_5 = -0.0042$	$b_5 = -0.0154$
$a_2 = 1.5610$	$b_2 = -0.1516$	$a_6 = 0.0009$	$b_6 = -0.0616$
$a_3 = -0.1826$	$b_3 = -0.0093$	—	—

Table A.5. Coefficients for the trigonometric interpolation for the nanowire superlattice SSL 3: $L_b = 0.93$ nm and $L_w = 3.64$ nm.

a_j (meV)	b_j (10^{-15} meV)	a_j (meV)	b_j (10^{-15} meV)
$a_0 = 70.7068$	—	$a_4 = 0.1581$	$b_4 = -0.0109$
$a_1 = -38.1334$	$b_1 = 0$	$a_5 = -0.0880$	$b_5 = -0.1460$
$a_2 = 3.2021$	$b_2 = -0.2660$	$a_6 = 0.0909$	$b_6 = 0.1281$
$a_3 = -0.5304$	$b_3 = 0.2838$	$a_7 = -0.0526$	$b_7 = -0.2232$

References

[1] Faist J, Capasso F, Sivco D L, Sirtori C, Hutchinson A L and Cho A Y 1994 Quantum cascade laser *Science* **264** 553–6
[2] Leo K 2003 *High-Field Transport in Semiconductor Superlattices* (*Springer Tracts in Modern Physics* vol 187) (Berlin: Springer)
[3] Bonilla L and Grahn H 2005 *Rep. Prog. Phys.* **68** 577–683
[4] Renk K F and Stahl B I 2011 *Phys. Lett.* A **375** 2644–51
[5] Lhuillier E, Péré-Laperne N, Rosencher E, Ribet-Mohamed I, Nedelcu A, Doyennette L and Berger V 2011 *Infrared Phys. Technol.* **54** 189–93
[6] Hicks L D and Dresselhaus M S 1993 *Phys. Rev.* B **47** 12727–31
[7] Shakouri A 2011 *Annu. Rev. Mater. Res.* **41** 399–443
[8] Terazzi R, Gresch T, Giovanni M, Hoyler N, Sekine N and Faist J 2007 *Nature Phys.* **3** 329–32
[9] Nagarajan R, Fukushima T, Corzine S W and Bowers J E 1991 *Appl. Phys. Lett.* **59** 1835–7
[10] Taghavi I, Kaatuzian H and Leburton J-P 2012 *Appl. Phys. Lett.* **100** 231114
[11] Wacker A 2002 *Phys. Rep.* **357** 1–111
[12] He Y, Hou D, Liu X, Han R and Chen J 2007 *IEEE Trans. Nanotechnol.* **6** 56–62
[13] Haug H and Jauho A-P 2008 *Quantum Kinetics in Transport and Optics of Semiconductors* 2nd edn (Berlin: Springer)
[14] Reich R K and Ferry D K 1982 *Phys. Lett.* **91A** 30–2
[15] Bonilla L and Escobedo R 2005 *Math. Models Methods Appl. Sci.* **15** 1253–72
[16] Kukuu A, Amano T, Karasawa T, Maeshima N and Hino K 2010 *Phys. Rev.* B **82** 115315
[17] Büttiker M and Thomas H 1977 *Phys. Rev. Lett.* **38** 78–80
[18] Kwok S H, Norris T B, Bonilla L L, Galán J, Cuesta J A, Martínez F C, Molera J M, Grahn H T, Ploog K and Merlin R 1995 *Phys. Rev.* B **51** 10171–4
[19] Hofbeck K *et al* 1996 *Phys. Lett.* A **218** 349–53
[20] Huang D, Lyo S and Gumbs G 2009 *Phys. Rev.* B **79** 155308
[21] Citrin D 2004 *Phys. Rev. Lett.* **92** 196803
[22] De Lima M *et al* 2010 *Phys. Rev. Lett.* **104** 165502
[23] Helm M, Hilber W, Strasser G, De Meester R and Peeters F M 1999 *Braz. J. Phys.* **29** 652–60
[24] Morandi O and Modugno M 2005 *Phys. Rev.* B **71** 235331
[25] Abramov I I, Goncharenko I A and Kolomeitseva N V 2007 *Semiconductors* **41** 1375–80
[26] Alvaro M and Bonilla L 2010 *Phys. Rev.* B **82** 035305
[27] Morandi O 2010 *Commun. Appl. Indus. Math.* **1** 167–84
[28] Holthaus M 1992 *Phys. Rev. Lett.* **69** 351–4
[29] Fomin V M and Kratzer P 2010 *Phys. Rev.* B **82** 045318
[30] Ktitorov S A, Simin G S and Sindalovskii V Ya 1971 *Fiz. Tverd. Tela* **13** 2230–3
Ktitorov S A, Simin G S and Sindalovskii V Ya 1972 *Sov. Phys.—Solid State* **13** 1872–4 (Engl. transl.)
[31] Ignatov A A and Shashkin V I 1987 *Zh. Eksp. Teor. Fiz.* **93** 935–43
Ignatov A A and Shashkin V I 1987 *Sov. Phys.—JETP* **66** 526–30 (Engl. transl.)
[32] Melnik R and He H 2000 *J. Eng. Math.* **38** 233–63
[33] Radulovic N *et al* 2006 *J. Comput. Theor. Nanosci.* **3** 551–9
[34] Bonilla L, Alvaro M and Carretero M 2011 *Phys. Rev.* B **84** 155316
[35] Perales A, Bonilla L and Escobedo R 2004 *Nanotechnology* **15** S229–33
[36] Arnold A 1996 *Commun. PDEs* **21** 473–506
[37] Schomburg E *et al* 1998 *Phys. Rev.* B **58** 4035–8
[38] Lhuillier E, Ribet-Mohamed I, Nedelcu A, Berger V and Rosencher E 2010 *Phys. Rev.* B **81** 155305
[39] Illner R, Zweifel P and Lange H 1994 *Math. Methods Appl. Sci.* **17** 349–76
[40] Lange H, Toomire R and Zweifel P 1995 *Rep. Math. Phys.* **36** 331–45
[41] Steinrück H 1991 *SIAM J. Math. Anal.* **22** 957–72
[42] Gerhardts R R 1993 *Phys. Rev.* B **48** 9178
[43] Yu R H 1993 *Phys. Rev.* B **47** 1379–82
[44] Abdallah N B and Mehats F 2005 *Commun. PDEs* **29** 173–206
[45] Abdallah N B, Castella F and Méhats F 2009 *SIAM J. Appl. Math.* **69** 1162–73
[46] Arnold A, Carrillo J A, Gamba I and Shu C S 2001 *Transport Theory Stat. Phys.* **30** 121–53
[47] Willatzen M *et al* 2004 *Math. Comput. Simul.* **65** 385–97
[48] Nakamura K, Shimizu A and Koshiba M 1991 *IEEE J. Quantum Electron.* **27** 2035–41
[49] Galeriu C *et al* 2004 *Comput. Phys. Commun.* **157** 147–59
[50] Costolanski A and Kelley C 2010 *IEEE Trans. Nanotechnol.* **9** 708–15